Geochimica et Cosmochimica Acta Vol. 50, pp. 2349–2361

0016-7037/86/$3.00 + .00

Dissolution at dislocation etch pits in quartz

SUSAN L. BRANTLEY*, STEPHANIE R. CRANE, DAVID A. CRERAR,
ROLAND HELLMANN and ROBERT STALLARD
Department of Geological and Geophysical Sciences, Princeton University, Princeton, NJ 08544, U.S.A.

(*Received August* 23, 1985; *accepted in revised form July* 16, 1986)

Abstract—Several samples of quartz were etched hydrothermally at 300°C in etchants of controlled dissolved silica concentration in order to measure the critical concentration, C_{crit}, above which dislocation etch pits would not nucleate on the quartz surface. C_{crit} for 300°C was theoretically predicted to be $0.6C_0$ and the measured C_{crit} was $0.75 \pm 0.15C_0$ (C_0 is the equilibrium concentration). Above this value, some dislocation etch pits formed, but the rate of formation significantly decreased. These results are the first experimental validation of etch pit formation theory under hydrothermal conditions. Dune sands showed a generally angular and pitted surface when etched in dilute solutions, while sands etched at $C \sim C_{crit}$ showed less angular pitting.

Analysis of a soil profile developed *in situ* on the Parguaza granite, Venezuela, revealed a gradual change from angular, pitted grain surfaces at the top of the profile to rounded surfaces on grains sampled just above bedrock. Since quartz dissolution without surface pitting continues deep in the profile, the Si concentration must exceed C_{crit} at depth.

These results indicate that for $C > C_{crit}$, dissolution occurs at edges and kinks on the surface of quartz and very few pits form; in contrast, at $C \ll C_{crit}$, dislocation etch pits grow rapidly, contributing to the overall dissolution rate.

LIST OF SYMBOLS

a	thickness of one molecular layer of quartz
A	frequency factor
b	Burgers vector of dislocation
C	concentration
C_{crit}	critical concentration predicted by Eqn. (7)
C_0	equilibrium concentration
ΔG_d	free energy of formation of a pit at a dislocation
ΔG_p	free energy of formation of a pit on a perfect surface
ΔG_v	volume contribution to free energy of formation of a pit
ΔG_s	surface contribution to free energy of formation of a pit
ΔG_d^*	activation barrier to opening of a pit at $C > C_{crit}$
J	pit nucleation rate
K	energy factor in Eqn. (5)
N	Avogadro's number
r	radius of pit
r_+, r_-	roots of Eqn. (5)
r_{crit}	critical radius of pit
r_0	dislocation core radius
R	gas constant
T	temperature
v_n	dissolution rate in a direction normal to the surface
v_s	dissolution rate in a direction parallel to the surface
V	molar volume
X_d	fraction of surface sites intersected by dislocations
γ	interfacial energy
τ	shear modulus
μ	chemical affinity
ν	Poisson ratio

INTRODUCTION

GEOCHEMISTS INTERESTED IN weathering and alteration processes have long recognized the need for a better understanding of the nature of the mineral surface and its influence on dissolution reactions. Identification of parabolic kinetics in the dissolution of feldspars by WOLLAST (1967) and later workers led to the development of dissolution models based on the formation of leached layers (see, for example, HELGESON, 1971). Experimental evidence has shown, however, that leached layers must be very thin (*e.g.* PETROVIC *et al.*, 1976) if they exist at all. Correlation between parabolic kinetics and presence of ultra-fine particles on the starting material (HOLDREN and BERNER, 1979) has led to a simple model of surface-controlled dissolution in which fine particles dissolve faster and cause apparent parabolic kinetics (PETROVIC, 1981a,b; HELGESON *et al.*, 1984). However, recent evidence from HOLDREN and SPEYER (1985a) shows that the dissolution rate is not directly proportional to surface area of fine particles, but instead may be proportional to concentration of active sites on the surface. Indeed, the most recent contribution to this controversy (CHOU and WOLLAST, 1984; HOLDREN and SPEYER, 1985b) has led to a theory of localized surface diffusion layers associated with non-uniformly distributed active sites (BERNER *et al.*, 1985). The importance of active site concentration in determining silicate dissolution kinetics was previously pointed out by LASAGA (1981), PETROVIC (1981a,b), and BERNER and coworkers (*e.g.* BERNER, 1978; BERNER *et al.*, 1980). Indeed, etch pits have been identified in many naturally dissolved samples (*e.g.* BERNER and SCHOTT, 1982; BERNER and HOLDREN, 1979) and have been used as evidence for interface-controlled dissolution. These poorly characterized "active sites" consist of dislocations, edges, microfractures, point defects, kinks, grain or twin boundaries, etc. (HELGESON *et al.*, 1984). We have investigated dissolution at dislocations intersecting the quartz surface (formation of etch pits) in an attempt to understand dissolution at one type of active site.

* *Present address:* Dept. of Geosciences, The Pennsylvania State University, University Park, PA 16802, U.S.A.

A further reason for studying dissolution at dislocations is that, although dislocation densities will rarely be large enough in crystals to cause higher equilibrium solubilities, the presence of high density dislocation tangles in deformed rocks can cause preferential dissolution and drive diffusive mass transfer (WINTSCH and DUNNING, 1985). A better understanding of the driving force for dissolution at dislocation outcrops is necessary in order to understand such strain-induced solution transfer.

Laboratory etching of crystals has long been used as a method to determine crystal symmetry and, more recently, as a method to count dislocation densities in solids (JOHNSTON, 1962). The actual process by which dislocations nucleate etch pits at the mineral surface, however, has not been extensively investigated. Theories for etch pit formation have been developed (CABRERA *et al.*, 1954; CABRERA and LEVINE, 1956; FRANK, 1951) and have been tested for some crystals (JOHNSTON, 1962). Application of these theories to geologically interesting materials may make it possible to use etch pit formation as a tool to interpret the nature of fluids interacting with mineral surfaces, as pointed out by LASAGA (1983) and LASAGA and BLUM (1986).

A major purpose of this paper is to test experimentally the existing theories for etch pit formation under geologically interesting conditions. We focus on the formation of etch pits at dislocation outcrops on the quartz surface. This paper summarizes our investigations concerning the role of dissolved silica concentration on the formation of etch pits under hydrothermal conditions where dissolution of quartz occurs at a measurable rate. We also discuss observations of etch pits on quartz particles from a soil profile in relation to pit nucleation theory.

THEORY

Dissolution can occur either at ledges on a crystal surface or by nucleation of dissolution pits. The driving free energy of pit nucleation consists of a volume energy term and a surface energy term:

$$\Delta G_p = \Delta G_v + \Delta G_s. \quad (1)$$

Formation of a pit in a perfect surface is slow because of the concomitant increase in surface area. It is the competition between the driving force for dissolution of a given volume (determined by the chemical affinity) and the increase in energy caused by forming more surface area which determines whether pit nucleation occurs. If the equilibrium solubility at temperature and pressure is C_0, and the dissolved concentration of the solid is C, then the chemical affinity is defined:

$$\Delta\mu = RT\ln(C/C_0) \quad (2)$$

where R is the gas constant and T is temperature in degrees Kelvin and activity corrections are neglected. For a pit approximated as a cylinder of depth a and radius r, the driving force for pit nucleation can be described (JOHNSTON, 1962):

$$\Delta G_p = \pi r^2 a(RT\ln(C/C_0))/V + 2\pi r a\gamma \quad (3)$$

where γ is the interfacial energy and V is the molar volume. Maximizing ΔG_p with respect to r yields the value of the critical radius for an etch pit on a perfect surface:

$$r_{crit} = -\gamma V/RT\ln(C/C_0). \quad (4)$$

This is the usual critical radius commonly referred to in nucleation theory and corresponds to the value at which ΔG_p goes through a maximum. For values of $r < r_{crit}$, the pit is unstable and should disappear, while for values of $r > r_{crit}$, pits should grow bigger. As the concentration of solute (C) increases, the critical radius also increases. The relationship between ΔG_p *vs.* r calculated for a perfect quartz surface at 300°C is illustrated in Fig. 1a. Details of the calculation are included in the discussion of Fig. 1b.

If instead of a perfect surface we assume a surface intersected by a dislocation, an additional strain energy term enters the driving force equation. Dissolution at

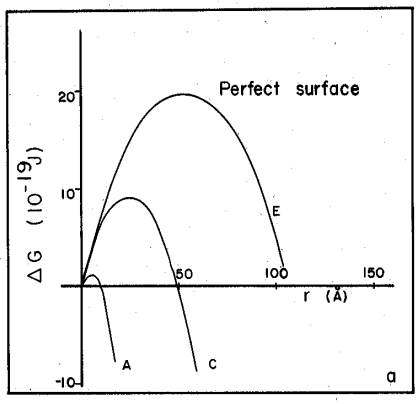

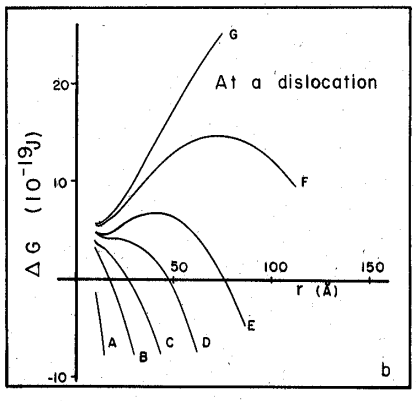

FIG. 1a. Calculated ΔG_p for pit nucleation on a perfect surface of quartz.

FIG. 1b. Calculated ΔG_d for pit nucleation at a dislocation on a quartz surface. Lettered curves correspond to the following Si concentrations: A ($0.04C_0$), B ($0.36C_0$), C ($0.51C_0$), D ($0.64C_0$), E ($0.73C_0$), F ($0.81C_0$), G ($0.89C_0$). Concentrations were chosen to correspond to selected experimental run conditions listed in Table 1.

a dislocation releases strain energy and favors pit formation. For a dislocation outcropping on a surface, FRANK (1951) and CABRERA and LEVINE (1956) used the following expression for the elastic energy in calculating the driving force:

$$\Delta G_d = \pi r^2 a(RT \ln (C/C_0))/ V + 2\pi r a\gamma - aKb^2(\ln (r/r_0))/4\pi \quad (5)$$

where K is an energy factor, b is the Burgers vector of the dislocation and r_0 is the dislocation core radius. In an isotropic material, the energy factor K is independent of dislocation orientation. For an edge dislocation in an isotropic material, $K = \tau/(1 - \nu)$, where τ is the shear modulus, and ν is the Poisson ratio. For a screw dislocation, $K = \tau$. For an anisotropic material such as quartz, K depends on the direction of both the dislocation and the Burgers vector.

Equation (5) neglects the core energy, which is important for values of r approximately equal to the Burgers vector (HIRTH and LOTHE, 1982). We can use the equation to calculate the free energy in enlarging the pit from a radius r_0 to a radius of r. For quartz at 300°C, using a shear modulus of $\tau \cong 0.48 \times 10^{11}$ Pa (HEINISCH *et al.*, 1975), a Burgers vector of 7.3 Å (HEINISCH *et al.*, 1975), γ = 360 mJ m^{-2} (PARKS, 1984), C_0 = 0.0097 m SiO_2 (WALTHER and HELGESON, 1977), and approximating the molecular height by $a = (V/N)^{1/3}$ where N is Avogadro's number, the ΔG_d of dissolution of a molecular layer can be calculated for values of C and r. Calculated ΔG_d values for a screw dislocation intersecting a quartz surface are plotted in Fig. 1b. For an edge dislocation, values of ΔG_d are calculated to be within 10% of that of a screw dislocation (ν for quartz = 0.077).

Note that no values have been calculated for $r < 7.3$ Å, which we have taken as an approximation of the dislocation core, r_0. Because linear elastic theory is not applicable close to the center of the dislocation, Eqn. (5) cannot predict the energy inside the dislocation core. As written, Eqn. (5) predicts that $\Delta G_d(r)$ goes to positive infinity as r approaches 0. This unphysical result can be remedied by adding a core energy term for $r < r_0$. An exact formulation of core strain energy has not been achieved, and we have not modeled it on Fig. 1. However, if an approximation for the core energy is included in Eqn. (5), ΔG_d is then constrained to go to 0 at $r = 0$. Inspection of Fig. 1 reveals that, if the calculation were to include a core energy term, ΔG_d would then exhibit another maximum for $r < r_0$. Choice of the value of r_0, as well as the form of the equation describing core energy, affects the topology of the ΔG_d function. LASAGA and BLUM (1986) discuss these effects and plot ΔG_d for various minerals and several assumed core radii.

As Fig. 1 shows, if a pit opens up at a dislocation because of the high core strain energy, the concentration of solute, C, determines whether there is an activation barrier to further outward dissolution of the pit. At a critical concentration C_{crit} (curve D), no activation barrier exists toward opening up of these angstrom-sized pits into observable etch pits. For concentrations $C > C_{crit}$ (curves E, F, G) an activation barrier does exist, and even if the core of the dislocation dissolves, opening of the pit into a macroscopic etch pit (> ~200 Å) is energetically unfavorable. This theory was tested in lithium fluoride, for which a critical concentration of $0.2C_0$ was measured (GILMAN *et al.*, 1958).

To determine the value of C_{crit}, we follow the derivation of CABRERA *et al.*, (1954, 1956) and maximize Eqn. (5) with respect to r and solve:

$$r = -r_{crit}/2[1 \pm (1 - Kb^2/2\pi^2\gamma r_{crit})^{1/2}]. \quad (6)$$

Values of r satisfying this equation will correspond to steady state solutions where the pit radius remains constant, while other parts of the crystal dissolves. The two roots of Eqn. (5), r_+ and r_-, correspond to maxima and minima of the ΔG_d function. Existence of a minimum in the free energy predicts that a hollow core can be stable (on Fig. 1, curves E, F, and G will exhibit minima very close to r = 10 Å). Note, however, that if the term $(Kb^2/2\pi^2\gamma r_{crit}) > 1$, there are no real solutions to Eqn. (6), and there is no steady state value of r; in this case, ΔG_d decreases steadily with r (curves A, B, C) and the pit should spontaneously open up to form a macroscopic etch pit. The critical concentration below which this occurs can be calculated by setting the above term equal to one and solving for C:

$$C_{crit} = C_0 \exp(-2\pi^2\gamma^2 V/RTKb^2). \quad (7)$$

At 300°C, the critical concentration for quartz with b = 7.3 Å is 0.62 C_0 (Fig. 1, curve D). A Burgers vector of 7.3 Å corresponds to a dislocation of direction $\langle c \pm a \rangle$. Although these type dislocations should be less common than those with b = 5.4 Å ($\langle c \rangle$) or b = 4.9 Å ($\langle a \rangle$), by choosing b = 7.3 Å, we calculate the upper limit for C_{crit} for observed dislocations (HEINISCH *et al.*, 1975; MCLAREN *et al.*, 1971). Error in the predicted C/C_0 for a given value of b is caused mainly by error in our choice of γ and K. PARKS (1984) estimates an error of about ±10% in the surface energy value; but, no data is available to correct γ for the effect of temperature. The value of K depends on dislocation direction, edge or screw character, and temperature. We estimate the error in the predicted C_{crit}/C_0 to be ±0.07.

Referring to Fig. 1, note that there is a free energy minimum (near r = 10 Å) and a maximum for all concentrations greater than C_{crit}. The difference of $\Delta G_d(r_-)$, the free energy minimum, and $\Delta G_d(r_+)$, the free energy maximum, corresponds to an activation energy barrier, ΔG_d^*, for etch pit formation. If a pit nucleates at a dislocation at $C > C_{crit}$, the pit should dissolve outward until $r = r_-$. Growth beyond this value is energetically unfavorable, and the nucleated pit should remain stable as a hollow core, without forming a macroscopic etch pit (see LASAGA and BLUM, 1986). Below C_{crit} there is no activation barrier to etch pit formation.

If we assume equilibrium for the size distribution of pit nuclei, the rate of formation of pits per unit area,

J, for concentrations above critical should have the form:

$$J = X_d A \exp(-\Delta G_d^*/RT) \quad (8)$$

where X_d is the fraction of surface sites intersected by dislocations and A is a frequency factor (HIRTH and POUND, 1963). Equation (8) and Fig. 1 show that formation of dislocation etch pits should be significantly slower above C_{crit}. As discussed earlier, including the core energy in Eqn. (5) would introduce an activation barrier for pit formation even for concentrations less than C_{crit}. If so, pit formation in highly undersaturated solutions would also show a rate dependence as in Eqn. (8), with a substantially smaller activation energy.

The production of shallow *versus* deep pits is controlled by the dissolution kinetics at the surface. If we consider a small idealized pit on the surface of a crystal (Fig. 2), we see that dissolution will occur in two directions: parallel to the surface, v_s, and normal to the surface, v_n. If $v_n > v_s$, a deep pit will form, whereas, if $v_s > v_n$, a shallow pit will form. A pit which nucleates at a surface point defect will have no driving force to cause a large v_n. At a dislocation the extension of the strained lattice into the crystal structure causes v_n to be very large, producing a deep etch pit or etch tube. If the crystal-solution interface energy is not isotropic, then v_s will be different depending on the crystallographic direction, producing a characteristic etch pit shape reflecting the crystal symmetry. Poisons, by adsorbing preferentially onto steps, can retard v_s and optimize the production of deep pits. Poisons may be essential to the formation of etch pits because they cause slow dissolution and help to maintain a large undersaturation at the surface, allowing etch pits to form (JOHNSTON, 1962).

Etch pits in quartz

WEGNER and CHRISTIE (1983) reviewed various etchants used to etch dislocations in quartz both at room temperature and hydrothermally. The correspondence between hydrothermally dissolved etch pits and dislocations has been demonstrated for the rhombohedral face $\{10\bar{1}1\}$ (JOSHI and VAG, 1968; JOSHI *et al.*, 1970), the prism face $\{10\bar{1}0\}$ (JOSHI and KOTRU, 1969), and the trigonal bipyramid face $\{11\bar{2}1\}$ (JOSHI and PAUL, 1977). These workers used distilled water or a concentrated NaOH solution to produce etch pits in synthetic quartz. They noted two types of etch features, deep pyramidal pits and shallow flat pits, produced by etching with distilled water on the rhombohedral face. By comparing etching on paired rhombohedral cleavage surfaces, they noted a "complete correspondence between the roughly pyramidal pits on both surfaces, both in regard to their number and in regard to position and size, while no relationship is observed for the flat and shallow pits" (JOSHI *et al.*, 1970, p. 85). They also noted that prolonged etching produced deeper pyramidal pits but caused the shallow triangular features to gradually disappear. They argued that these results suggest that the shallow flat-bottomed pits correspond to a surface defect while the pyramidal pits are caused by line defects. HICKS (1985) describes these same features for hydrothermally etched natural quartz.

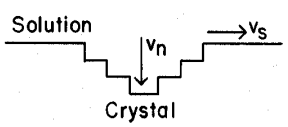

FIG. 2. Schematic cross-section of a dissolving etch pit on the crystal surface. Dissolution rate along the surface is noted by v_s; dissolution rate normal to the surface is noted by v_n.

The shape and size of etch pits in quartz is crystallographically controlled and etchant specific (WEGNER and CHRISTIE, 1983). Shape of etch pits is controlled by the relative dissolution rates in different crystallographic directions, just as final crystal shapes are determined by relative rates of growth in different directions. ERNSBERGER (1960) has discussed factors controlling dissolution rates on quartz as a function of crystal direction. Hydrothermal etch pits on the rhombohedral face of quartz are characteristically pyramidal, with triangular bases uniformly oriented with respect to the crystal. In these pyramidal pits, the apex of the pit lies along the dislocation line, and the center of the base of the pyramid indicates the original intersection of the dislocation with the surface. The symmetry of the etch pit is determined by the angle of the line defect with respect to the surface and the anisotropy of the surface energy. Since the bulk of a natural crystal is formed by growth on the major and minor rhombohedral faces, these faces are characterized by dislocations oriented within 30° of the perpendicular to the surface (LANG and MIUSCOV, 1967).

EXPERIMENTAL METHOD

Two different types of experiments were run, using three different starting materials (Table 1). In the first set of experiments, we placed cut pieces of Arkansas quartz crystals with 50 ml of silica solution in standard sealed autoclaves in a temperature-controlled oil bath (described by WOOD *et al.*, 1984). These "closed" experiments were run at saturated vapor pressure at 300°C or 200°C (±10°C) for 6.5 hours. In the second set of experiments, starting material was placed in a flow-through chemical reactor (POSEY-DOWTY *et al.*, 1986) in order to maintain a constant chemical affinity throughout the experiment. The reactor was then heated to 300°C ± 8° and a Si solution was pumped through at a rate of 0.7 ± 0.1 ml/min at 1250 ± 100 psi. Flow-through experiments were run using cut pieces of Arkansas quartz, dune sand grains and half pieces of doubly terminated quartz crystals from Herkimer County, N.Y. (Herkimer diamonds, available from Wards Scientific Supply, Inc.)

In all experiments with Arkansas quartz, the crystal pieces were cored normal to the rhombohedral face. Each individual run used crystal pieces from the same crystal face (R1–R5, R9) or the same crystal (R7, R8). Dune sand was chosen as a second substrate in order to examine pitting on naturally rounded surfaces. The Herkimer diamonds were used to study pitting on crystal faces other than $\{10\bar{1}1\}$. After completion of the experiments, crystals were coated with Au-Pd and observed by SEM. Several of the etched crystal pieces were cleaned of their Au-Pd coating (as described by HICKS, 1985), and re-etched. These runs are denoted by the notation SE in

Table 1. Experimental Run Conditions and Results

Run No.	Start Concen. Si (m)	Start Concen. Na(m)	Final[1] Concen.(m) Si(m)	Temp. (°C)	Press.[2] (psi)	Etch time (h)[3]	Pit Density (cm^{-2})	Statistical Uncertainty
Closed Runs (Arkansas quartz):								
R1S1	0.0020	0.001	0.0083	298*2	Sat.	6.5	1.9×10^{5}	2×10^{4}
R1S2	0.0040	0.002	0.0084	298	Sat.	6.5	2.9×10^{5}	3×10^{4}
R1S4	0.0081	0.004	0.012	298	Sat.	6.5	9×10^{3}	5×10^{3}
R1S5	0.010	~0.005	0.014	298	Sat.	6.5	9×10^{3}	5×10^{3}
R2S1	0.0069	0.007	0.011	305*5	Sat.	6.5	3.6×10^{4}	1×10^{4}
R2S2	0.0080	0.008	0.010	305	Sat.	6.5	2.1×10^{4}	9×10^{3}
R2S4	0.0097	0.016	0.012	305	Sat.	6.5	2×10^{4}	8×10^{3}
R2S5	0.012	0.016	0.014	305	Sat.	6.5	9×10^{3}	5×10^{3}
R3S1	0.0021	0.002	0.0053	300*2	Sat.	6.5	1.2×10^{6}	6×10^{4}
R3S2	0.0042	0.004	0.0072	300	Sat.	6.5	3.0×10^{5}	3×10^{4}
R3S3	0.0064	0.003	0.013	300	Sat.	6.5	9.9×10^{4}	2×10^{4}
R3S4	0.0085	0.004	0.010	300	Sat.	6.5	$<3\times10^{3}$	-
R4S1	0.0	0.0	0.0001	206*1	Sat.	6.5	$<3\times10^{3}$	-
R4S2	0.0008	0.001	0.001	206	Sat.	6.5	2.7×10^{4}	9×10^{3}
R4S3	0.0015	0.002	0.0026	206	Sat.	6.5	3×10^{3}	3×10^{3}
R4S4	0.0030	0.003	0.0030	206	Sat.	6.5	6×10^{3}	4×10^{3}
R4S5	0.0041	0.005	0.0048	206	Sat.	6.5	9×10^{3}	5×10^{3}
Flow Runs (Arkansas Quartz):								
R5S1	0.0079	0.0	0.008	295*5	2200*200	6.5	2.3×10^{3}	7×10^{2}
R5S1SE	0.0079	<.0001	0.009	300*2	1250*20	31.5	1.2×10^{3}	5×10^{2}
R5S2	0.0071	0.0	0.007	300*2	1200*20	6.5*	1.2×10^{4}	1×10^{3}
R5S2SE	0.0080	0.0005	0.009	300*5	1250*20	31.5	2.1×10^{3}	7×10^{2}
R5S3	0.0058	<.0001	0.006	300*2	1200*20	6.5	1.4×10^{4}	2×10^{3}
R5S3SE	0.0073	0.00042	0.008	300*2	1250*20	31.5	1.8×10^{4}	2×10^{3}
R5S4	0.0052	<.0001	0.005	300*2	1200*100	6.5	2.3×10^{4}	3×10^{3}
R5S5	0.0050	-	0.005	300*2	1200*20	6.5	1.7×10^{4}	2×10^{3}
R5S5SE	0.0053	0.0002	0.005	300*2	1250*20	31.5	4.6×10^{4}	4×10^{3}
R5S6	0.0035	-	0.003	300*2	1200*20	6.5	3.1×10^{4}	3×10^{3}
R5S7	0.0	0.0	0.0001	300*2	1200*100	6.5	10^{4}-10^{5}	-
R5S7SE	0.0	0.0	<.004	300*2	1250*20	31.5	-	-
R9S1	0.0087	0.0005	.008-.01**	300*2	1200*20	28.0	1.2×10^{4}	2×10^{3}
R9S1SE	0.0079	<.0001	0.0085	300*2	1250*20	53.0	9.7×10^{3}	1×10^{3}
R9S2	0.0087	0.0005	.008-.01**	300*2	1250*20	5+	7×10^{3}	1×10^{3}
R9S2SE	0.0079	<.0001	0.0085	300*2	1250*20	30+	5×10^{3}	1×10^{3}
R9S4	0.0073	0.0004	0.008	300*2	1250*20	25.0	6.1×10^{4}	4×10^{3}
Flow Runs (Herkimer Diamonds):								
R7S1	0.0062	0.0002	0.006	300*3	1250-800	6.5	-	-
R7S2SE	0.0042	-	0.004	300*2	1200*100	13.0	-	-
R8S1	0.0073	0.0002	0.008	300*3	1280*30	53+	2×10^{3}	2×10^{3}
R8S2	0.0079	0.00005	0.0085	300*2	1250*20	25.0	-	-
R12S1	0.0073	0.0002	0.008	300*3	1280*30	53+	6.3×10^{3}	1×10^{3}
Flow Runs (Dune Sand):								
R11S1	0.0023	0.0001	-	297*3	1100*20	25	-	-
R11S2	0.007	0.0003	-	300*2	1100*20	25	-	-

Footnotes

1. Final dissolved Si concentration for static experiments; average Si concentration during run for flow experiments
2. Sat. = Saturated vapor pressure at run temperature
3. Total etching time for a sequentially - etched crystal (labeled SE)

* Run interrupted, cooled, and started again because of clogging
** Si concentration varied during run between values indicated
\+ Run stopped flowing during experiment, estimated flow time is indicated

Table 1. Re-etching is necessary to ascertain that shallow surface defects not associated with line defects dissolve away (WEGNER and CHRISTIE, 1983). Two samples, from crystals R5 and R9, were also cut, polished, argon ion-thinned, and analyzed for dislocations under TEM.

Silica solutions were prepared according to the method of CRERAR *et al.* (1981). All solutions were adjusted to pH 7 at 25°C with NaOH. Solution samples were taken before and after the static experiments, and continuously during the flow-through experiments. Si and Na (present as an artifact of the preparation procedure) were analyzed by ICP.

RESULTS

Table 1 lists the experimental runs and observations. In addition, Figs. 3 and 4 record features observed and noted in Table 1 and the discussion. All rhombohedral faces were examined for deep, crystallographically controlled point-bottomed pits. These pits correspond to the "roughly pyramidal" pits of JOSHI *et al.* (1970) and are associated with dislocations. Shallow, flat-bottomed pits were also noted on most samples (Fig. 3). In general, the distribution of pits was very inhomogeneous. In some cases, small etch pits within larger, flat-bottomed pits, associated with stepped or branching dislocations (JOSHI *et al.*, 1978) were observed. In sample R5S5SE and R9S4 we also observed very deep polygonal-shaped etch holes centered on triangular pits (see also HICKS, 1985). Observations of etching on the three starting materials are summarized below.

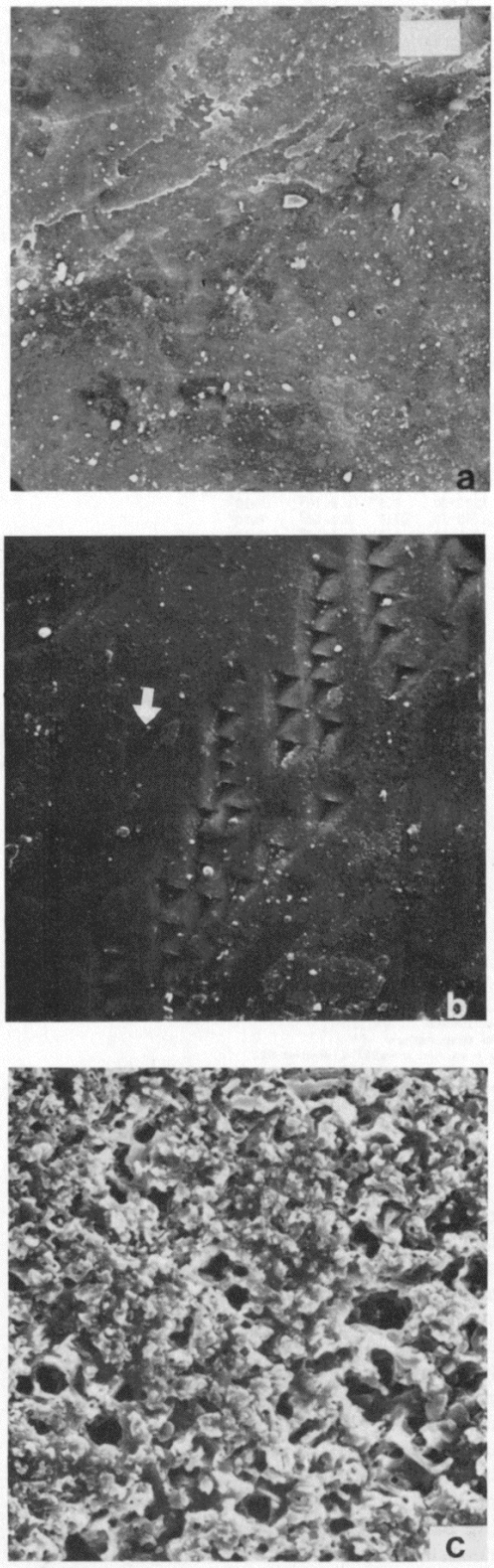

FIG. 3. SEM photomicrograph of characteristic etch features on quartz surface etched 31.5 hours at different Si concentrations. Scale in all photos is the same: scale bar = 10 microns. a) Sample R5S1SE, C = 0.0079 m. b) Sample R5S3SE, C = 0.0073 m. Note shallow triangular features (white arrow), and more distinct deep triangular features. c) Sample R5S7SE, C = 0.0 m.

Arkansas quartz

In order to quantify the presence of pits on the rhombohedral face, etch pit counts were made for runs 5 and 9. Each measurement consisted of a count of deep etch pits on a randomly selected surface sample imaged at 1000× under SEM. Although distinguishing shallow pits from deep pits was difficult for the short etch period experiments, we attempted to count only deep pits with etched apexes, excluding pits with flat bottoms. Figure 3a is an example of a surface exhibiting no deep etch pits and a few barely recognizable shallow triangular features. Figure 3b shows examples of both deep and shallow etch figures. At least forty such counts were made for each crystal, and the calculated pit densities (number of pits observed/total area) are listed in Table 1, along with error estimates. Pit densities counted for unreacted samples from crystal R5 and R9 were $1 \times 10^4 \pm 2 \times 10^3$ cm^{-2} and $2 \times 10^3 \pm 1 \times 10^3$ cm^{-2}, respectively. Data from R1–R4 based on fifteen counts at 1000× reported by CRANE (1985) are also listed. Pit densities for unreacted samples from R1, R2, and R3 were $3 \times 10^3 \pm 3 \times 10^3$ cm^{-2}, and for R4 were $2 \times 10^4 \pm 8 \times 10^3$ cm^{-2}. Unetched surfaces of samples R2 and R9 were generally rougher than the other crystals.

Results from runs R1–R3, R5 and R9 are plotted in Fig. 5. Measured pit densities for R4, run at 200°C, were at background levels and are not plotted. For quartz etched with distilled water, etch pits were very small and difficult to count (R5S7) or the surface was so extremely etched that no triangular pits were discernible (R5S7SE, Fig. 3c) and are also not plotted. Densities are plotted as average pit density ± estimated error (discussed later) *versus* saturation index, C/C_0. C_0 was given the value of 0.0097 m (WALTHER and HELGESON, 1977). Analytical error for silica concentration was ±5%, as plotted in Fig. 5b for the flow experiments. In most cases, the variation in silica concentration for the flow experiments was within this analytical uncertainty during the run. Although silica concentration increased throughout the closed runs, only starting concentrations have been noted on Fig. 5a. The critical concentration at 300°C as calculated earlier for a Burgers vector of 7.3 Å is also plotted.

For both the closed and flow runs, there is a clear decrease in measured pit density with increasing saturation index, C/C_0, although pit densities in the closed runs were generally higher than comparable flow runs. For runs R1–R3 and R5, essentially no pits were observed above $0.8C_0$. Pit density in R9 was substantially higher than R5, and crystal R9S1, etched at $0.9C_0$

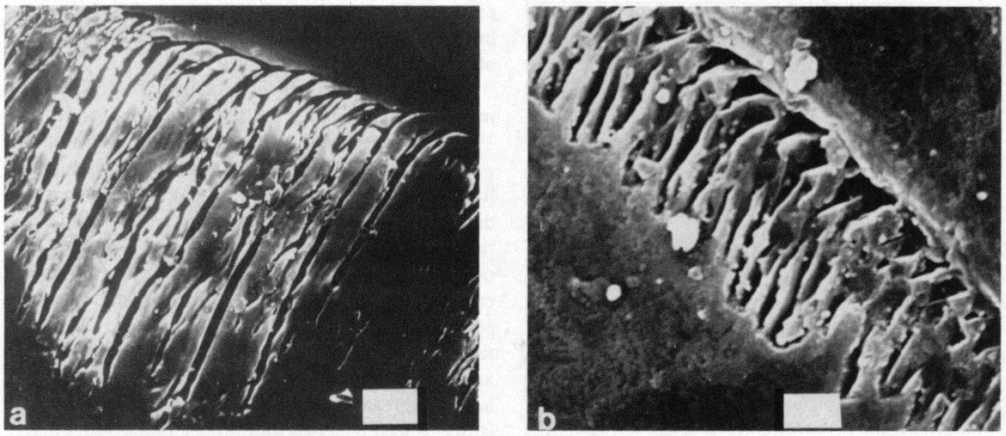

FIG. 4. SEM photomicrographs of characteristic arcuate etching on quartz surfaces. a) Sample R5S2, etched 6.5 hours at $C = 0.0071$ m. Scale bar = 5 microns. b) Sample R5S6, etched 6.5 hours at $C = 0.0035$ m. Scale bar = 1.7 microns.

showed significant pitting. The unreacted surface of R9 was also much rougher than the surface of R5.

TEM on crystals R5 and R9 revealed dislocation densities on the order of 10^6 cm^{-2}. Results of TEM tilting experiments using the simple isotropic invisibility criterion (see WENK, 1976) on dislocations in R5 and R9 revealed several dislocations with Burgers vectors of the $\langle a \rangle$ orientation, and other dislocations which were either $\langle a \rangle$ or $\langle c + a \rangle$. No extensive identification of Burgers vectors was made due to the low dislocation density and the rapid damaging of the quartz foil by the electron beam. All dislocations observed were close to perpendicular to the face, and, in general, groups of dislocations found together in a sample always had the same orientation and the same Burgers vectors.

Herkimer diamonds

Three Herkimer diamonds (R7, R8, R12) were etched in order to investigate etching on faces other than the rhombohedral. The minor rhombohedral or z $\{01\bar{1}1\}$ face generally showed triangular etch pits similar to those of the r face. The $\{11\bar{2}1\}$ or s face showed both triangular and diamond-shaped pits, as described by HICKS (1985). The prismatic faces showed no consistently identifiable pit morphology. We did not make pit density counts on these faces because of their small size and inconsistent shape. Etching on the rhombohedral faces produced features as described for the Arkansas quartz crystals: shallow, flat-bottomed etch triangles were observed to be very prevalent, and very difficult to distinguish from point-bottomed pits, except for the very longest etch times (*i.e.* R8S1, R12S1). For that reason, only etch pit counts for runs R8S1 and R12S1 have been included in Table 1.

Sand grains

The two experiments with dune sand yielded surfaces characterized by both etching and precipitation. The precipitated cover made observation of the etched surfaces difficult. However, etching by a dilute solution for 25 hours (R11S1) produced a more angularly pitted surface than etching with a solution nearer saturation (R11S2). No clearly distinguishable crystallographically controlled etch figures were observed.

DISCUSSION

Figure 5 shows that between $0.7C_0$ and $0.9C_0$ (0.007 m to 0.009 m), all etch pit densities reached background levels. The statistical error estimates for the pit density measurements tabulated in Table 1 were made assuming a Poisson distribution. The pit density, calculated as the total number of counted pits, x, divided by the total imaged area, should have a standard deviation equal to $x^{1/2}$/area. The statistical error of Table 1 corresponds to one standard deviation of the data. Plotted error bars in Fig. 5 are liberal estimates of error including all systematic problems as discussed below. Note that the observed decrease in etch pit densities with increasing C/C_0 is well above our estimated error.

There are several sources for systematic error in our measurements. The most obvious is the inhomogeneous distribution of dislocations in a crystal, which can cause variation in the expected density of dislocation etch pits. Etch pits were often observed to be associated in linear groups, as shown in Fig. 3b. We believe that these areas could be examples of the high dislocation densities characteristic of polygonal growth cell boundaries observed by x-ray topography for $(10\bar{1}1)$ quartz slices (LANG and MIUSCOV, 1967). Another cause of inhomogeneous pit dissolution could be non-ideal flow inside the reactor which would cause pooling or stagnation of fluid and inhomogeneous dissolution. We performed our etch pit counts by randomly selecting areas distributed across the surface in order to sample the entire dissolved area.

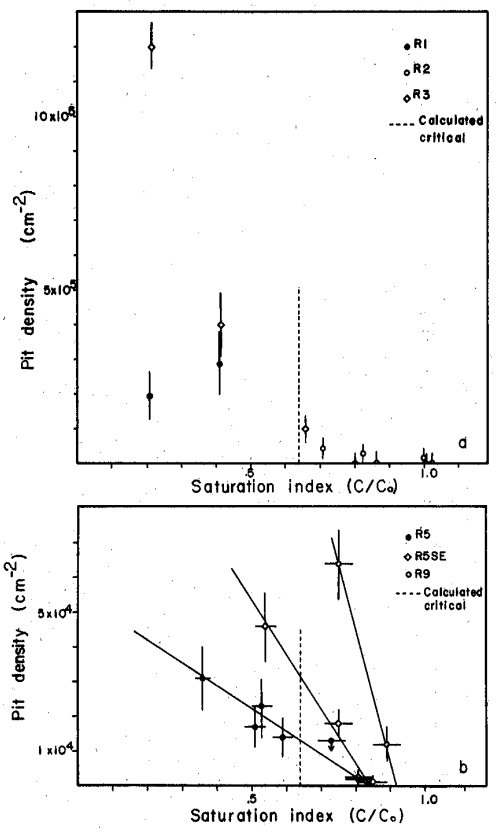

FIG. 5a. The effect of dissolved Si starting concentration (expressed as the ratio C/C_0) on etch pit density measured on crystal surfaces etched for 6.5 hours in sealed autoclaves. Labels refer to runs listed in Table 1.

FIG. 5b. The effect of dissolved Si concentration (expressed as the ratio C/C_0) on etch pit density measured on crystal surfaces etched for 6.5 hours (R5), 31.5 hours (R5SE), and 25–28 hours (R9) in a chemical flow reactor. Samples plotted as R5SE were cleaned, re-etched samples from R5 (Table 1). R9 was a different crystal. A least-squares fit to the flow data has been plotted in order to determine where pit densities reach background levels.

The etch pit counts themselves were difficult to execute mainly due to the small pit size, especially for the 6.5 hour flow runs. Longer etch periods produced less ambiguous and larger etch figures, although overlap of large etched triangles sometimes obliterated individual pits. Comparison of pit densities measured for different magnifications often yielded varying apparent densities, since smaller pits are lost at lower magnifications; a magnification of 1000× was chosen for all runs. Even at 1000×, the subjectivity of determining deep *vs.* shallow pits added to the error. Indeed, the difference in absolute value of pit densities in the closed experiments (R1–R3) calculated from CRANE (1985) and the flow experiments (R5–R9) is at least partly due to the subjectivity of different experimenters in counting of pits; however, the closed experiments did produce deeper more well-developed pits which may have been related to higher Na concentrations or lack of stirring.

Another problem was the presence of "arcuate etching" on the rhombohedral face (Fig. 4 and see HICKS, 1985). The curved, sometimes nested, nature of the etching and the linearity of some of the features suggests that surface scratches and micro-cracks with associated dislocations may control some of these dissolution features. As the solute concentration drops below C_{crit} in our experiments, the central linear portion of the arcuate etching shows characteristic deep etch pits with curved edges (Fig. 4b). These features are similar to the "beaked pits" summarized by JOHNSTON (1962) and thought to be caused by dissolution of impurity haloes (segregated impurities lying within the strained lattice caused by a dislocation). Etch pits with curved edges, associated with these linear features, were not counted in the flow experiment pit density counts.

Several replicate counts were made on representative samples. Reproducibility was found to be within $\pm 1\sigma$ as noted in Table 1. In several counts, we also included "curved" etch pits (see Fig. 4b) and other pits associated with linear features, in order to compare to our reported pit densities. In these cases our counts were within 3σ of the quoted results. As a very liberal estimate of our systematic error, we have plotted our data in Fig. 5 with error bars equaling three times the statistical error of Table 1. Despite these large error estimates, there is a clear decrease in pit density with increasing saturation index.

Although the TEM provided only rough dislocation counts, it is apparent that not all dislocations produced etch pits. The increase in pit densities on sequentially etched surfaces showed that pits were still nucleating on the surface during the time scale of our experiments. Sequential experiments in which the rate of etch pit formation is followed for different silica concentrations would be the best way to determine the value of C_{crit}. By plotting log (rate) *vs.* log $(C/C_0)^{-1}$ as suggested by Eqn. (8), a break in slope should occur at C_{crit}. Although our data on sequentially etched crystals is too limited to warrant the calculation of rates, we observed that for $C > 0.8C_0$, observed pit densities either decrease or remain the same (R5S1, R5S2, R9S1, R9S2), and for $C < 0.8C_0$, pit densities increase (R5S3, R5S5) with time.

The observed decrease in etch pit density in some sequentially etched samples is probably due to overcounting of etch pits for short period etchings where shallow and deep pits are not always distinguishable. Evidence for this comes from R8, in which two halves of a Herkimer diamond were run in separate experiments at $C \sim 0.0075$ m. After 25 hours, the rhombohedral face from one half was covered with triangular etch figures, both shallow and deep (R8S2). Estimating the etch pit density of the face ($\sim 10^4$ cm^{-2}) was difficult because shallow pits hadn't dissolved away. After 53 hours the etch pit density of the other half crystal was clear, because shallow and deep pits were easily distin-

guishable. The density was quite low: 2×10^3 cm^{-2} (R8S1).

The observed differences in absolute value of pit density for different crystals etched under similar conditions could be related to starting dislocation densities, the character of the dislocations present in different crystals (edge *vs.* screw, Burgers vector), or the impurity content. TEM did not reveal any differences in dislocation densities in R5 and R9 and we did not complete enough tilting experiments to see any difference in measured Burgers vectors for the two samples. The only other possible explanation is the observation that the unreacted surface of R9 was rougher than that of R5. HICKS (1985) and CRANE (1985) both noted that rough surface layers, with anomalous etching features, were present on some crystals. These layers would presumably reflect different growth conditions, including temperature effects or impurity concentrations, of the crystal. A higher prevalence of arcuate etching on R9 also suggests that impurity concentrations in R9 were different than R5. There is some evidence that aluminum impurity can influence the roughness of a surface (LANG and MIUSCOV, 1967).

The combined results of all runs support three general observations. First, etch pits form on quartz at a significantly reduced rate at 300°C when solution concentrations reach $0.8C_0$. Second, etch pit densities decrease gradually with increasing saturation index, rather than dropping off as a step function at one critical concentration. Third, some etch pits are observed on surfaces of quartz etched above $0.8C_0$.

The first observation allows an estimation of C_{crit}: our best estimate at 300°C is 0.0078 m ± .0007 m SiO_2, which corresponds to $0.80 \pm 0.07C_0$, using WALTHER and HELGESON's (1977) value of 0.0097 m for C_0. If we use FOURNIER and POTTER's (1982) value of 0.011 m for C_0, our estimated $C_{crit} = 0.7C_0$, which is closer to the theoretically predicted C_{crit} of $0.62 \pm 0.07C_0$ (b = 7.3 Å). Combining the uncertainty in our data and in C_0, our best experimental estimate is $C_{crit} = 0.75 \pm 0.15C_0$ at 300°C.

Our TEM work suggests that most of the dislocations which intersect the r face of R5 and R9 have $\langle a \rangle$ or $\langle c \pm a \rangle$ Burgers vectors. Because there are two or more Burgers vectors, there will be a range in critical concentrations, explaining the observed decrease of etch pit density with increasing saturation index. Although our data suggests that C_{crit} (experimental) > C_{crit} (theoretical), it is unlikely that $b > 7.3$ Å for the etched dislocations. MCLAREN *et al.* (1971) report that only three types of dislocations are common ($b = \langle a \rangle, \langle c \rangle, \langle c \pm a \rangle$), and it is theorized that dislocations of larger Burgers vector would dissociate into less-strained dislocations of unit Burgers vector.

The observation of pits forming even as C approaches C_0 could indicate that the surface energy of the quartz-water interface at 300°C is lower than that of 25°C, or that impurities segregated in the dislocations have perturbed the local surface energy. An alternate interpretation is that, at 300°C, even with a nucleation barrier present ($C > C_{crit}$), dissolution is rapid enough that some pits form. This would correspond to a large frequency factor in Eqn. 8. Our data cannot distinguish between these two possibilities.

Etch tubes

Polygonal-shaped etch holes centered on triangular etch pits were observed for samples R5S5SE and R9S4 (see also HICKS, 1985). We believe that these features correspond to the etch tunnels of NIELSEN and FOSTER (1960). LANG and MIUSCOV (1967) review other observations of etched tunnels, and report that HF etching of a piece cut parallel to an r plane of a synthetic crystal produced etch tunnels in about one third of all dislocations imaged by x-ray topography. LANG and MIUSCOV also report the formation of etch tunnels along dislocations in natural crystals. Impurity segregation has been suggested as an explanation for the enhancement of v_n at these dislocations.

The formation of long needlelike etch tubes suggests an attractive hypothesis for formation of syngenetic fluid inclusions (WILKINS and MCLAREN, 1981). Indeed, NIELSEN and FOSTER (1960) point out that synthetic quartz crystals often trap long fluid inclusions which formed as etched tubes in the seed crystal during autoclave heat-up. In rocks, it seems likely that permeating fluids would etch tunnels along dislocations, which if later sealed off, would ovulate into fluid inclusions (as described in SMITH and EVANS, 1984). In deformation zones where dislocation densities as high as 10^{11} cm^{-2} have been reported, this process would allow the incorporation of fluid inclusions and promote access of water into grain interiors.

NATURAL ETCH PITS

The observation that pits form at very high saturation levels of the fluid calls into question LASAGA's (1983) original idea that the presence of etch pits on a mineral surface could be used to determine dissolved concentrations of the paleo-fluids, at least in hydrothermal systems. The utility of such analysis for interpretation of surfaces of weathered grains, or other crystals altered in low temperature environments, however, is still possible. At lower temperatures, Eqn. (7) predicts a lower C_{crit} to C_0 ratio, so C_{crit} would be significantly lower than C_0.

Etch pits on sediment quartz grains have been documented for several depositional environments by various workers (see KRINSLEY and DOORNKAMP, 1973). Surfaces are characterized by a mixture of features which have been attributed to mechanical abrasion, chemical precipitation, and dissolution. The *in situ* weathering environment on the other hand is characterized by grains generally from the same source and unabraded by transport. *In situ* soil grain surface features can then be attributed solely to chemical processes. Etch pits have been documented for various minerals in the weathering environment (BERNER and HOLDREN, 1979; BERNER and SCHOTT, 1982). We analyzed the surfaces of quartz soil particles from an *in*

situ soil profile to test whether etch pit formation was controlled by chemistry of the percolating fluids.

The soil we analyzed was sampled from a 1 m thick soil profile 20 km south of Puerto Ayacucho, Venezuela (STALLARD, 1984). The profile developed *in situ* on the Parguaza granite, an Early Proterozoic rapikivi granite of the Guyana Shield (GAUDETTE *et al.*, 1978). Samples were collected at intervals from bedrock to the surface. Titanium and zirconium enrichment in the soil indicates that just below the surface, 90% of the original bedrock material had been removed by dissolution. Quartz grains were isolated by treating each sample with 1 M hydroxylamine hydrochloride in 25% (v/v) acetic acid to dissolve amorphous ferromanganese minerals (CHESTER and HUGHES, 1967). This was followed by fusion of the residue in pre-heated sodium pyrosulfate and dissolution in hydrofluosilicic acid which had been pre-equilibrated with quartz (KIELY and JACKSON, 1964; JACKSON *et al.*, 1976). These procedures remove phyllosilicates and some feldspars and have been shown to yield nearly 100% recovery of quartz (JACKSON *et al.*, 1976). In addition, SEM analysis revealed the presence of a large number of fine grains and clean cleavage surfaces, indicating that the

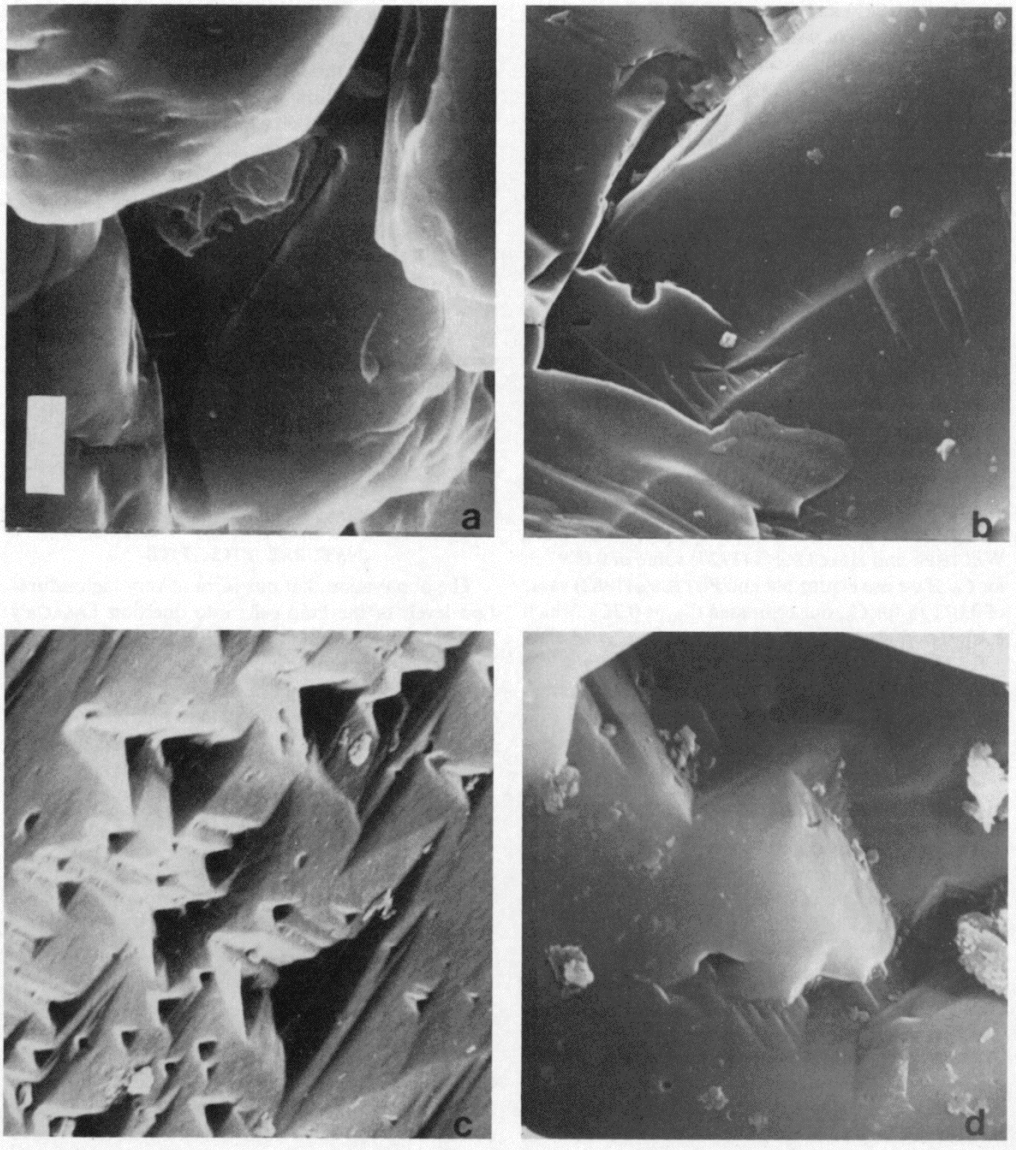

FIG. 6. SEM photomicrographs of characteristic surface features of sand grains from soil profile developed *in situ* on the Parguaza granite, Venezuela. Scale bar = 2.5 microns. a) Sample from 2 cm, just above bedrock. b) Sample from 90 cm deep. c) Sample from 60 cm deep. d) Sample from surface.

chemical treatment did not attack the quartz grains. The quartz surface features are solely a result of weathering processes.

We found that surface morphologies of the naturally weathered sand grains show an interesting pattern of etching as a function of depth (Fig. 6). Photos show characteristic surface morphologies from quartz grains from the bottom (just above bedrock), middle (90 cm and 60 cm deep), and top of the profile. The observation of pitting which changes as a function of depth suggests that the existence of etch pits is controlled by some depth-related factor. The quartz/Ti ratios for bedrock, and for samples a, b, c, and d in Fig. 6 are 210, 180, 130, 63, and 37, respectively. These observations, corroborated by the presence of rounded grains at the base of the profile, indicate that quartz dissolution is continuing at all depths. The observation of triangular etch pits, very similar to those observed in our single crystal experiments and in HICKS' (1985) sand dissolution experiments, suggests that our results at high temperature may be applicable toward interpretation of dissolution at lower temperatures. As fluid passes through the profile, silica dissolves from the soil grains pushing the silica concentration toward saturation. Our experiments at high temperature suggest that the concentration of silica could control the pitting. It appears that deeper than 60 cm in the profile silica concentrations are higher than C_{crit} at 25°C, so that surfaces are not pitted (Fig. 6a, b). Instead, at these depths, dissolution occurs at corners and edges producing rounded grains. A more thorough investigation of chemical etching as a function of soil depth and fluid chemistry should give further clues to the fluid history in the weathering environment.

CONCLUSIONS

Our experiments show that as quartz dissolves a critical concentration of dissolved silica is reached above which etch pits are formed on the surface at a significantly reduced rate. This effect is predicted by the theory of FRANK (1951) and CABRERA and LEVINE (1956). Using literature values for the various quartz parameters, a C_{crit} of $0.62C_0$ is predicted at 300°C. This is within the estimated error of the measured C_{crit} of $0.75 \pm 0.15C_0$. Although the measurement of an exact value for C_{crit} is difficult, we can use the estimate to calculate the quartz-water surface energy: $\gamma = 280 \pm 90$ mJ m^{-2}. More accurate measurements of pit formation rates would allow a better measurement of the quartz-water interfacial energy.

Under hydrothermal conditions, the rate of pit formation above C_{crit} is dramatically reduced, although crystals etched in hydrothermal solutions can show etch pits even when $C > C_{crit}$. Interpretation of etch pits on hydrothermally dissolved quartz surfaces will not unequivocally reveal saturation levels of the reactant fluids. However, surfaces exhibiting etch pits formed at low temperature may indicate $C < C_{crit}$ of the reactant fluids. As an example of this effect, we observed that etch pit densities on quartz surfaces from a soil profile decrease with depth, which we interpret to be caused by the increase in Si concentration in pore fluids. More research is necessary to completely interpret the nature of pits and density of pits on natural surfaces with respect to silica concentration.

Enhanced dissolution at dislocation outcrops should also be important in strain-driven solution transfer. Previous analyses of strain-enhanced dissolution (WINTSCH and DUNNING, 1985) have focused on the increased "equilibrium" solubility of a highly strained crystal. The localized effect summarized in this paper would enhance dissolution in strained areas of a crystal. This work further shows that once $C > C_{crit}$, nucleation at dislocations slows dramatically, implying that in open systems where C is maintained below critical, solution attack should be more aggressive than in closed systems. The etching of needlelike tubes along dislocations also provides a mechanism by which water can enter deformed mineral grains, which may help to explain the noted correlation of dislocations with fluid inclusions (*e.g.* ORD and CHRISTIE, 1984). This process would also greatly affect the mechanical properties of the etched grains.

It would be interesting to extend such work to other crystals, as well as to relate pit formation to bulk crystal dissolution. For $C > C_{crit}$, dissolution occurs at edges and kinks on the surface and very few pits form; in contrast, at $C \ll C_{crit}$, pits form rapidly, contributing to the overall dissolution rate. The noted correlation between surface-controlled dissolution and etch pits most likely results from concentrations $C < C_{crit}$ due to slow surface reaction kinetics. The ubiquity of etch pits on naturally dissolved mineral grains has been noted (VELBEL, 1984); however, the relative importance of pit nucleation rates in determining silicate dissolution and reaction kinetics remains to be demonstrated. From such studies will come a more fundamental understanding of mineral dissolution processes ranging from low temperature weathering reactions to alteration reactions occurring under hydrothermal conditions.

Acknowledgements—Analysis of the soil profile and much of the hydrothermal work was completed by S. R. Crane as her senior thesis at Princeton University. We appreciate the help of Maria Borscik, Elaine Lenk, and Laurel Pringle-Goodell for help with chemical, SEM, and TEM analysis, respectively. The TEM work would not have been possible without the generosity of RCA scientists Dr. Marvin Abrahams and Chuck Buiocchi who allowed us to use their argon ion-thinner. This work was funded by NSF grant #EAR-82-18726 and #EAR-84-19421. D.A.C. gratefully acknowledges support from the Shell Companies Foundation. Work by R.F.S. in Venezuela is supported by the Venezuelan Ministerio del Ambiente y Recursos Naturales Renobales, by a Dusenbery Preceptorship, and N.S.F. grant #EAR-84-07651. This manuscript benefitted from reviews by M. A. Velbel, A. C. Lasaga, and W. Casey.

Editorial handling: G. R. Holdren, Jr.

REFERENCES

BERNER R. A. (1978) Rate control of mineral dissolution under earth surface conditions. *Amer. J. Sci.* **278**, 1235–1252.

BERNER R. A. and HOLDREN G. R. (1979) Mechanism of feldspar weathering—II. Observations of feldspars from soils. *Geochim. Cosmochim. Acta* **43,** 1173–1186.

BERNER R. A. and SCHOTT J. (1982) Mechanism of pyroxene and amphibole weathering II. Observations of soil grains. *Amer. J. Sci.* **282,** 1214–1231.

BERNER R. A., SJOBERG E. L., VELBEL M. A. and KROM M. D. (1980) Dissolution of pyroxenes and amphiboles during weathering. *Science* **207,** 1205–1206.

BERNER R. A., HOLDREN G. R. and SCHOTT J. (1985) Surface layers on dissolving silicates. *Geochim. Cosmochim. Acta* **49,** 1657–1658.

CABRERA N. and LEVINE M. M. (1956) On the dislocation theory of evaporation of crystals. *Phil. Mag.* **1,** 450–458.

CABRERA N., LEVINE M. M. and PLASKETT J. S. (1954) Hollow dislocations and etch pits. *Phys. Rev.* **96,** 1153.

CHESTER R. and HUGHES M. J. (1967) A chemical technique for the separation of ferromanganese minerals, carbonate minerals and adsorbed trace elements from pelagic sediments. *Chem. Geol.* **2,** 249–262.

CHOU L. and WOLLAST R. (1984) Study of the weathering of albite at room temperature and pressure with a fluidized bed reactor. *Geochim. Cosmochim. Acta* **48,** 2205–2217.

CRANE S. R. (1985) The role of the critical concentration in etch pit formation during dissolution of quartz. Senior thesis, Dept. Geological and Geophysical Sciences, Princeton University.

CRERAR D. A., AXTMANN E. V. and AXTMANN R. C. (1981) Growth and ripening of silica polymers in aqueous solutions. *Geochim. Cosmochim. Acta* **45,** 1259–1266.

ERNSBERGER F. M. (1960) Structural effects in the chemical reactivity of silica and silicates. *J. Phys. Chem. Solids* **13,** 347–351.

FOURNIER R. O. and POTTER R. W. (1982) An equation correlating the solubility of quartz in water from 25°C to 900°C at pressures up to 10,000 bars. *Geochim. Cosmochim. Acta* **46,** 1969–1974.

FRANK F. C. (1951) Capillary equilibria of dislocated crystals. *Acta Cryst.* **4,** 497–501.

GAUDETTE H. E., MENDOZA V., HURLEY P. M. and FAIRBARN H. W. (1978) Geology and age of the Parguaza rapakivi granite, Venezuela. *Geol. Soc. Amer. Bull.* **89,** 1335–1340.

GILMAN J. J., JOHNSTON W. G. and SEARS G. W. (1958) Dislocation etch pit formation in lithium fluoride. *J. Appl. Physics* **29,** 747–754.

HEINISCH H. L. JR., SINES G., GOODMAN J. W. and KIRBY S. H. (1975) Elastic stresses and self-energies of dislocations of arbitraty orientation in anisotropic media: olivine, orthopyroxene, calcite and quartz. *J. Geophys. Res.* **80,** 1885–1896.

HELGESON H. C. (1971) Kinetics of mass transfer among silicates and aqueous solutions. *Geochim. Cosmochim. Acta* **35,** 421–469.

HELGESON H. C., MURPHY W. M. and AAGAARD P. (1984) Thermodynamic and kinetic constraints on reaction rates among minerals and aqueous solutions. II. Rate constants, effective surface area, and the hydrolysis of feldspar. *Geochim. Cosmochim. Acta* **48,** 2405–2432.

HICKS B. D. (1985) Quartz dissolution features: An experimental and petrofabric study. Masters thesis, University of Missouri-Columbia.

HIRTH J. P. and POUND G. M. (1963) *Condensation and Evaporation: Nucleation and Growth Kinetics,* New York: MacMillan Co.

HIRTH J. P. and LOTHE J. (1982) *Theory of Dislocations.* John Wiley and Sons, New York.

HOLDREN G. R. and BERNER R. A. (1979) Mechanism of feldspar weathering—I. Experimental studies. *Geochim. Cosmochim. Acta* **43,** 1161–1171.

HOLDREN G. R. and SPEYER P. M. (1985a) Reaction rate surface area relationships during the early stages of weathering—I. Initial observations. *Geochim. Cosmochim. Acta* **49,** 675–681.

HOLDREN G. R. and SPEYER P. M. (1985b) pH dependent change in the rates and stoichiometry of dissolution of an alkali feldspar at room temperature. *Amer. J. Sci.* **285,** 994–1026.

JACKSON M. L., SAYIN M. and CLAYTON R. (1976) Hexafluorosilicic acid reagent modification for quartz isolation. *Soil Soc. Amer. J.* **40,** 958–960.

JOHNSTON W. G. (1962) Dislocation etch pits in non-metallic crystals. *Prog. Ceramic Science* **2,** 3–75.

JOSHI M. S. and VAG A. S. (1968) Application of the selective etch method in the study of structural defects in synthetic quartz. *Sov. Phys.-Cryst.* **12,** 573–580.

JOSHI M. S. and KOTRU P. N. (1969) Hydrothermal etching of matched fractured prism faces of quartz. *Sov. Phys.-Cryst.* **14,** 427–428.

JOSHI M. S. and PAUL B. K. (1977) Surface structures of trigonal bipyramid faces of natural quartz crystals. *Amer. Mineral.* **62,** 122–126.

JOSHI M. S., KOTRU P. N. and ITTYAKHEN M. A. (1970) Studying dislocations in quartz by the hydrothermal-etching method. *Sov. Phys.-Cryst.* **15,** 83–89.

JOSHI M. S., KOTRU P. N. and ITTYAKHEN M. A. (1978) Revelation of stepped dislocations in amethyst crystals by hydrothermal etching. *Amer. Mineral.* **63,** 744–746.

KIELY P. V. and JACKSON M. L. (1964) Quartz feldspar and mica determination for soils by pyrosulfate fusion. *Soil Sci. Amer. Proc.* **29,** 159–163.

KRINSLEY D. H. and DOORNKAMP J. C. (1973) *Atlas of Quartz Sand Surface Textures.* Cambridge U. Press, Cambridge.

LANG A. R. and MIUSCOV V. F. (1967) Dislocations and fault surfaces in synthetic quartz. *J. Appl. Phys.* **38,** 2477–2483.

LASAGA A. (1981) Rate laws of chemical reactions. In *Kinetics of Geochemical Processes* (ed. A. LASAGA and R. J. KIRKPATRICK), *Reviews in Mineralogy, Vol. 8,* pp. 1–110. Mineral. Soc. Amer.

LASAGA A. (1983) Kinetics of silicate dissolution. 4th International Symposium on Water-Rock Interaction, Extended Abstracts, Misasa, Japan.

LASAGA A. C. and BLUM A. E. (1986) Surface chemistry, etch pits and mineral-water reactions. *Geochim. Cosmochim. Acta* **50,** 2363–2379 (this issue).

MCLAREN A. C., OSBORNE C. F. and SAUNDERS L. A. (1971) *Phys. Stat. Sol.* (a) **4,** 235–247.

NIELSEN J. W. and FOSTER F. G. (1960) Unusual etch pits in quartz crystals. *Amer. Mineral.* **45,** 299–310.

ORD A. and CHRISTIE J. M. (1984) Flow stresses from microstructures in mylonitic quartzites of the Moine Thrust zone, Assynt area, Scotland. *J. Struct. Geo.* **6,** 639–654.

PARKS G. A. (1984) Surface and interfacial free energies of quartz. *J. Geophys. Res.* **89,** 3997–4008.

PETROVIC R. (1981a) Kinetics of dissolution of mechanically comminuted rock-forming oxides and silicates. I. Deformation and dissolution of quartz under laboratory conditions. *Geochim. Cosmochim. Acta* **45,** 1665–1674.

PETROVIC R. (1981b) Kinetics of dissolution of mechanically comminuted rock-forming oxides and silicates. II. Deformation and dissolution of oxides and silicates in the laboratory and at the Earth's surface. *Geochim. Cosmochim. Acta* **45,** 1675–1686.

PETROVIC R., BERNER R. A. and GOLDHABER M. B. (1976) Rate control in dissolution of alkali feldspars—I. Study of residual feldspar grains by X-ray photoelectron spectroscopy. *Geochim. Cosmochim. Acta* **40,** 537–548.

POSEY-DOWTY J., CRERAR D., HELLMANN R. and CHANG C. (1986) Kinetics of mineral-water reactions: I. Theory, design and application of circulating hydrothermal equipment. *Amer. Mineral.* **71,** 85–94.

SMITH D. L. and EVANS B. (1984) Diffusional crack healing in quartz. *J. Geophys. Res.* **89,** 4125–4135.

STALLARD R. F. (1984) River chemistry, geology, geomorphology, and soils in the Amazon and Orinoco Basins. In *The Chemistry of Weathering,* (ed. J. I. DREVER), pp. 293–316. D. Reidel Publ. Co.

VELBEL M. A. (1984) Weathering of Minerals. In *MAC Short Course in Environmental Geochemistry*, (ed. M. E. FLEET), pp. 67–111, Miner. Assoc. Canada.

WALTHER J. V. and HELGESON H. C. (1977) Calculation of the thermodynamic properties of aqueous silica and the solubility of quartz and its polymorphs at high pressures and temperatures. *Amer. J. Sci.* **277**, 1315–1351.

WEGNER M. W. and CHRISTIE J. M. (1983) Chemical etching of deformation substructures in quartz. *Phys. Chem. Minerals* **9**, 67–78.

WENK H.-R. (ed.) (1976) *Electron Microscopy in Mineralogy.* Berlin: Springer-Verlag.

WILKINS R. W. T. and MCLAREN A. C. (1981) The formation of syngenetic fluid inclusions from etch pits in crystals. *N. Jb. Miner. Mh.* **5**, 221–224.

WINTSCH R. P. and DUNNING J. (1985) The effect of dislocation density on the aqueous solubility of quartz and some geologic implications: A theoretical approach. *J. Geophys. Res.* **90**, 3649–3657.

WOLLAST R. (1967) Kinetics of the alteration of K-feldspar in buffered solutions at low temperature. *Geochim. Cosmochim. Acta* **31**, 635–648.

WOOD S. A., CRERAR D. A., BRANTLEY S. L. and BORCSIK M. (1984) Mean molal stoichiometric activity coefficients of alkali halides and related electrolytes in hydrothermal solutions. *Amer. J. Sci.* **284**, 668–705.